ADVANCED FUNCTIONAL MATERIALS
www.afm-journal.de

Solvent-Mediated Reconstruction of the Metal–Organic Framework HKUST-1 ($Cu_3(BTC)_2$)

*Gerardo Majano, Oliver Martin, Markus Hammes, Stef Smeets, Christian Baerlocher, and Javier Pérez-Ramírez**

The principle of integral metal–organic framework (MOF) reconstruction is demonstrated for differently degraded HKUST-1 via a facile, one-step, solvent-assisted treatment. Controlled MOF degradation by exposure to 77% humidity, liquid water, and diluted hydrochloric acid produces a mixture of non-porous crystalline hybrid materials containing protonated linker and copper-oxo species, which are then reconstructed back into high-quality HKUST-1 by contacting them with ethanol. X-ray diffraction and sorption kinetics reveal a true memory effect of the system from completely degraded materials. The reconstruction approach is consequently extrapolated to gas- and liquid-phase treatments in a fixed-bed reactor with ethanol and ethanol/water mixtures for use in CO_2 capture from a simulated pre-combustion gas stream. Up to a maximum of 94% porosity and 85% CO_2 sorption capacity can be recovered from a steamed material. A degradation-reconstruction model is put forward based on X-ray diffraction observations and structural analyses, microscopy, N_2 sorption, thermogravitry–mass spectrometry and IR spectroscopy observations, particularly elucidating the influence of various degradation pathways on the reconstruction.

1. Introduction

Metal–organic frameworks (MOFs) are innovative materials built out of metal nodes and organic ligands forming extended, crystalline porous structures. They exhibit remarkable properties (high surface area, defined metal sites, and accessible porous structure), which remain unmatched for prospective applications in gas sorption, separation, catalysis and biomedicine.[1–6] Nevertheless, up to date their industrial scope has barely breached scaled-up syntheses of a handful of structures. As a result of the characteristic ionic and flexible nature of their framework, the most significant barrier for MOF application has been their hydrothermal stability,[7] which directly impacts the final stage of their life cycle. While the stability of some MOF structures can reach temperatures up to 500 °C (e.g., Al–benzenedicarboxylate[8] and ZIF-8),[9] extensive research has been focused on delaying their so-far inevitable degradation, with special interest on water-related effects. Explored approaches include use of mixed linkers,[10] hydrophobization of the linker,[11] variation of the framework through functionalization,[12–14] encapsulation of polyoxometalates,[15] isolation of crystals from humidity by carbon layers,[16] generation of interpenetrated structures[17] and theoretical work on the effect of solvent coordination.[18] Unfortunately most of these routes raise the operational cost or they are not amenable for industrial application. Thus, a general optimization for any selected application by removing water or just finding a compromise between the present of water and a certain degradation degree of the MOF material remains as the only viable route for fighting or minimizing its deterioration by humidity.

In spite of some reports presenting a rather integral approach for MOF application,[19] the final and critical step of MOF lifetime has been largely ignored. While porous aluminosilicate materials such as zeolites do not present practically any hazard after their lifetime is exhausted, spent MOF materials would result in a potentially problematic mixture of metallic and aromatic compounds, which would require expensive solvent extraction and work-up. This poses financial and ecological issues deterring their adoption into industrial applications and underlines the urgent need for material recovery strategies after their degradation.

A general mechanistic picture of MOF degradation by water has been known for quite some time.[7] Basically, water molecules gradually coordinate the metal nodes, structurally weakening the framework with increasing coordination and ligand displacement.[20] Finally, this results in the complete hydrolysis of the metal-linker bond followed by the collapse of the framework, resulting in a material containing the protonated (carboxylic) linker and the metal hydroxide.[7,21–23] Such a degradation path has also been verified for HKUST-1 ($Cu_3(BTC)_2$, BTC = 1,3,5-benzenetricarboxylate) in the presence of water during the sorption of ammonia in the gas phase and under steaming of polyoxometalate-containing materials.[15,24]

Dr. G. Majano, O. Martin, Dr. M. Hammes, Prof. J. Pérez-Ramírez
Institute for Chemical and Bioengineering
Department of Chemistry and Applied Biosciences
ETH Zurich, Vladimir-Prelog-Weg 1,
CH-8093, Zurich, Switzerland
E-mail: jpr@chem.ethz.ch
S. Smeets, Dr. C. Baerlocher
Laboratory of Crystallography
ETH Zurich, Vladimir-Prelog-Weg 5, CH-8093, Zurich

DOI: 10.1002/adfm.201303678

HKUST-1 is a highly efficient and versatile material for reversible CO_2 sorption[25] possessing moderate steam stability,[7] which has been recently synthesized through the transformation of a layered metal hydroxide, $Cu(OH)_2$.[26] Additionally, it was shown for the case of Fe-BTC that the hydroxide precursor needs to possess a flexible and accessible layered structure in order to stimulate its conversion into a MOF material.[27] The favorable acid-base interaction between the linker and the basic metal hydroxide resulted for both cases in the conversion occurring at room temperature after only a few minutes. This effect drastically increases productivity and lowers related costs by avoiding the use of high temperatures and additional process steps. Considering such a remarkable interaction, it is feasible to postulate the reversibility of the degradation of the MOF porous network via hydrolysis and to question whether the intimate nature of the resulting mixture of metal species and linker can indeed override the need for a layered ordering in the hydroxide. Herein, we report for the first time that the degradation of the MOF porous network can be reversible and exhibits a true memory effect using HKUST-1. This is demonstrated utilizing diverse batch degradation-reconstruction experiments, which were extrapolated, in liquid and gas phase, to a continuous fixed-bed reactor setup for their application in CO_2 capture. This result constitutes a fine complementary process to the very interesting surface effects of solvent-assisted merging of single crystals into larger ones, which has been very recently reported as a method for healing mechanically-induced fractures on MOF/polydimethylsiloxane composite materials.[28] Furthermore, the presented approach demonstrates decisive advantages over templated recrystallization methods,[29] overcoming limitations such as the dependence on templating additives, reliance on dissolved species and the liquid phase, and the inevitable blockage of accessible porosity; thus making it not only more effective, but also amenable to industrial application, with especial emphasis on gas capture. The consequences of this finding are significant, as it may boost the changes for large-scale application of HKUST-1 by addressing crucial concerns of material lifetime, reconditioning and recovery.

2. Results and Discussion

2.1. Batch Degradation and Reconstruction

Table 1 summarizes all the samples prepared in this study, their specific treatment conditions, and sorptive properties. In a preliminary experiment, a pristine amount of HKUST-1 (sample P) was stored in a 77% relative humidity atmosphere at room temperature (sample RH). After more than two months, the porous network was completely collapsed into a hybrid material, which has been reported[24] to consist of trimesic acid (TA, 1,3,5-benzenetricarboxylyic acid) and diverse copper-oxo species. The change was accompanied by a marked transition in color, from vivid to light blue (see **Figure 1**), the latter characteristic of $Cu(OH)_2$. Upon contacting the obtained degraded material with ethanol at room temperature under stirring, a great part of the original structure of HKUST-1 could be reconstructed within 1 h (see **Figure 2**, sample RH-EtOH-1 h). Taking into account that the collapse of the HKUST-1 pore network is caused by hydrolysis, it was also plausible to expect that a dehydration of the resulting non-porous material could lead to a reconstruction of HKUST-1. Even so, dehydration experiments in vacuum (100 °C during 3–48 h and 150 °C during 16 h) were not successful in recovering the HKUST-1 structure (Supporting Information, Figure S1), which is in agreement with previously reported observations.[30] Both of these results pointed towards the need of a minimal amount of solvent in order to provide certain flexibility for the structure to be reconstructed. However, compared to template-assisted recrystallization methods,[29] no significant dissolution of species was observed in this work. While the speed of the reconstruction for this initial experiment was remarkable, the large amount of time required for obtaining the deteriorated MOF material made this approach rather impractical for our study. Thus, for the development of kinetic studies, accelerated degradation of HKUST-1 was applied. This was achieved by direct treatment of HKUST-1 in water (samples W) or aqueous 0.1 M HCl (samples H) at 85 °C under stirring for periods ranging from 30 min to 4 h. As expected, HCl treatment showed certain dissolution of the material but soluble species were separated by filtration and washing. Since no additional remarkable changes were observed in the X-ray diffraction patterns of both samples (Supporting Information, Figure S2) after treatment for 30 min, these were used for further evaluation and experiments. Exhibiting a lower signal intensity, the diffraction patterns of the obtained samples were not only different between

Table 1. Treatment conditions and sorption properties of samples studies.

Sample	Treatment conditions	S_{BET} [$m^2\ g^{-1}$]	Mean crystal size [μm]
P	–	1716 /1470[a)]	0.380
RH	77% relative humidity, 2.5 months	11	1.6
W	H_2O, 85 °C, 30 min	93	17
H	HCl, 85 °C, 30 min	16	33
RH-EtOH	EtOH, 25 °C, 1 h	963	0.625[b)]
W-EtOH	EtOH, 25 °C, 5 min–72 h	88–421	2.5[b)]
H-EtOH	EtOH, 25 °C, 5 min–72 h	30–965	0.035[b)]
S	N_2:H_2O = 50:50, 275 °C, 2 h	161	0.394
S-g-EtOH	N_2:EtOH = 50:50, GHSV[c)] = 700 h^{-1}, 5 h, 90 °C	224	0.326
S-g-EtOH-H_2O	N_2:EtOH:H_2O = 50:25:25, GHSV[c)] = 700 h^{-1}, 5 h, 90 °C	920	0.377
S-l-EtOH-H_2O	Volumetric EtOH:H_2O = 50:50, LHSV[d)] = 0.72 h^{-1}, 5 h, 70 °C	1340	0.384

[a)]pelletized; [b)]1 d; [c)]gas-hourly space velocity; [d)]liquid-hourly space velocity.

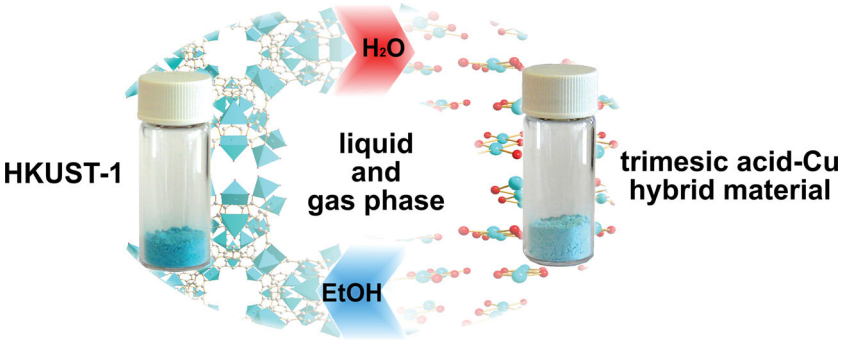

Figure 1. Solvent-assisted reconstruction of water-degraded HKUST-1 (right) back into the original material (left) is accompanied by a rapid, characteristic change in colour.

these two degradation methods but also from sample RH. Water treatment led to a crystalline material with a densification of the structure. Taking into account that the degradation process could eventually entail the formation of diverse crystalline phases, structure solutions were attempted using powder diffraction patterns collected with synchrotron radiation (details in the Experimental Section). Although all samples investigated appeared to consist of more than one phase, fortunately, sample H could be fully analyzed and it can be considered as a model for the partial decoordination of TA and formation of layers. It consists of 2 phases, denoted H1 and H2, the last one being the major phase (ca. 85%).

The two structures are depicted in **Figure 3**. In both, the 3-dimensional framework structure is lost and basically differ only in the number of acid groups per TA molecule that are coordinated to Cu. In H1, each TA molecule has two carboxyl groups coordinated to a Cu atom, which leads to 1-dimensional zigzag coordination TA:Cu polymer chain with a TA:Cu ratio of 1:1. In H2, on the other hand, only one carboxyl group per TA is coordinated to a Cu atom, resulting in a molecule with two TA and one Cu (TA:Cu ratio of 1:0.5). The Cu atom has a square pyramidal coordination geometry in H1, and a square planar one in H2. In both structures, the Cu is coordinated to two O atoms of different TA molecules in a *trans* arrangement. Since H2 is the main phase, the total TA:Cu ratio is close to 1:0.5, containing less Cu than in the parent material (1:1.5). Upon treatment with ethanol, only sample H experienced a favorable reconstruction, recovering about half of the crystallinity (and half of the previous total surface area, vide infra) after 1 day. Sample W remains almost unaltered after 1 day (Figure 2, right, and Figure S5). It should consist of at least three phases, phase H1 of this report, a phase identified as a layered $[Cu_2OH(TA)(H_2O)]$ compound,[31] and a major phase which could not yet be solved (see the Experimental Section). However, the remaining Bragg peaks can be indexed with a monoclinic cell that has also a cell parameter of 3.5 Å, indicating also a layered structure.

The entire process was also followed by scanning electron microscopy (SEM) imaging. The degradation of HKUST-1 via different methods results in marked morphology changes (Figure 2, insets). Predominantly, the original morphology of

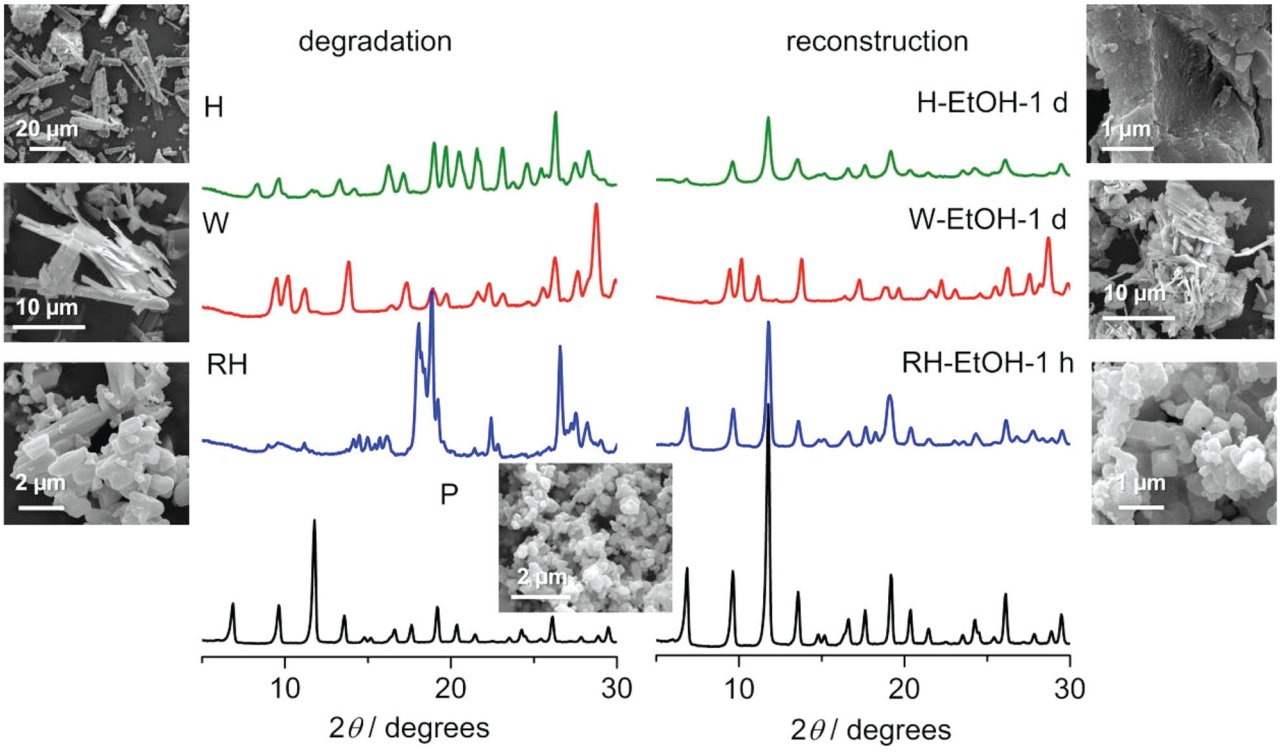

Figure 2. X-ray diffraction patterns and scanning electron micrograph (insets) of HKUST-1 samples upon degradation via different methods and the resulting reconstruction products. The parent HKUST-1 diffractogram on the degradation side has been scaled down 3 times.

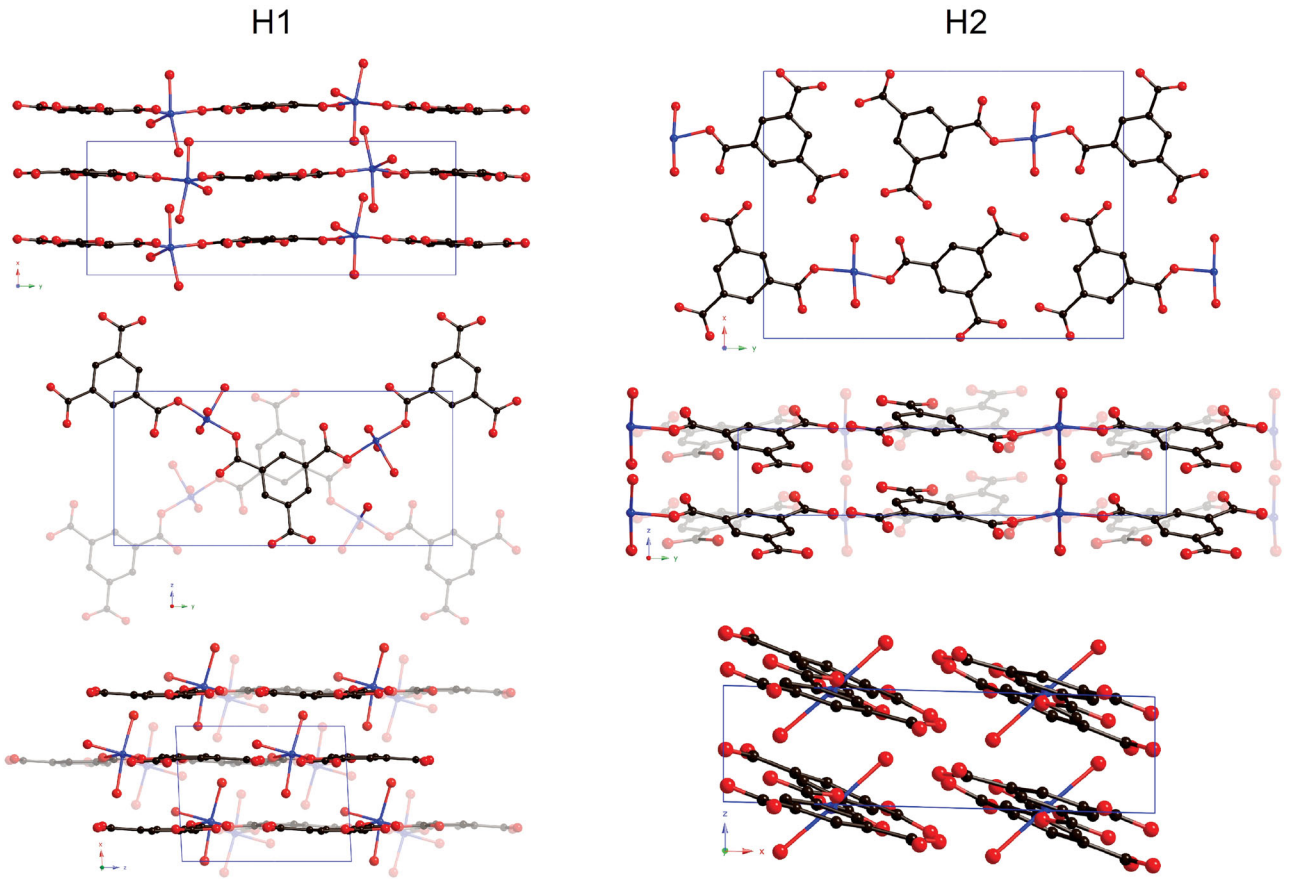

Figure 3. Crystal structures of H1 and H2 phases along the *z*-axis (top), *x*-axis (middle) and *y*-axis (bottom). Fading is used to indicate depth.

sub-micrometer-sized octahedral crystals with narrow size distribution was replaced by multi-micron, layered crystals, which strongly resembled the precursor $Cu(OH)_2$. The humidity-produced sample RH showed smaller size and less defined crystalline features. With liquid treatments, the size of the crystals increased to more than 10–20 µm and their features became more defined. However, the samples treated with HCl showed rougher features due to corrosion of the crystal, which is in line with X-ray diffraction (XRD) results. Upon reconstruction, a broader particle size distribution of octahedral crystals was observed. This can easily be explained by the crystalline layered structure of the precursor degraded material acting as a growth matrix for HKUST-1. Such an effect has previously been reported, where it limited the size and controlled the size distribution of the crystals.[26] In the case of reconstruction, the crystal size distribution broadened due to the expected increase in disorder of the layers, general crystalline structure of the precursor and presence of diverse phases. Sample W showed no remarkable change, but only a reduction in crystal size and some agglomeration after contact with EtOH for 1 day. Longer treatments up to 3 days did not significantly alter the crystalline features.

Nitrogen sorption of the samples complemented structural XRD observations and enabled a closer monitoring of the reconstruction kinetics. The porosity of the parent HKUST-1 (S_{BET} = 1716 m^2 g^{-1}) was completely lost upon degradation of most samples and presented a total surface area of only 11 m^2 g^{-1} for sample RH (**Figure 4**a). As expected, the initial mild conditions of degradation of the experiment with sample RH led to a material with faster reconstruction kinetics resulting in the recovery of 50% porosity (S_{BET} = 963 m^2 g^{-1}) in 1 h (Figure 4a). The detailed S_{BET} evolution using samples W and H (Figure 4b) demonstrated the difference in the reconstruction of the obtained structures. The material treated with HCl exhibited faster kinetics, outperforming the water-treated sample.

Assessment of the evolution of N_2 isotherms (**Figure 5**a and Supporting Information Figure S6) revealed that, similarly to the MOF synthesis from $Cu(OH)_2$,[26] there is a rapid evolution of the microporosity accompanied by the generation of some textural porosity in the form of a strong hysteresis effect at high relative pressure. This transient textural porosity declined with the evolving reconstruction. An effect that can be related to the opening of the layers of the degraded crystals through HKUST-1 octahedral crystals, as observed in SEM images of sample H-EtOH, just 5 min into the reconstruction treatment (Figure 5b). The crystalline features in the false-colored SEM also support the notion that dissolution does not play an important role in the reconstruction phenomenon, as if it was otherwise, segregated agglomerates of HKUST-1 would be observed alongside corroded crystals of the degraded material. Although

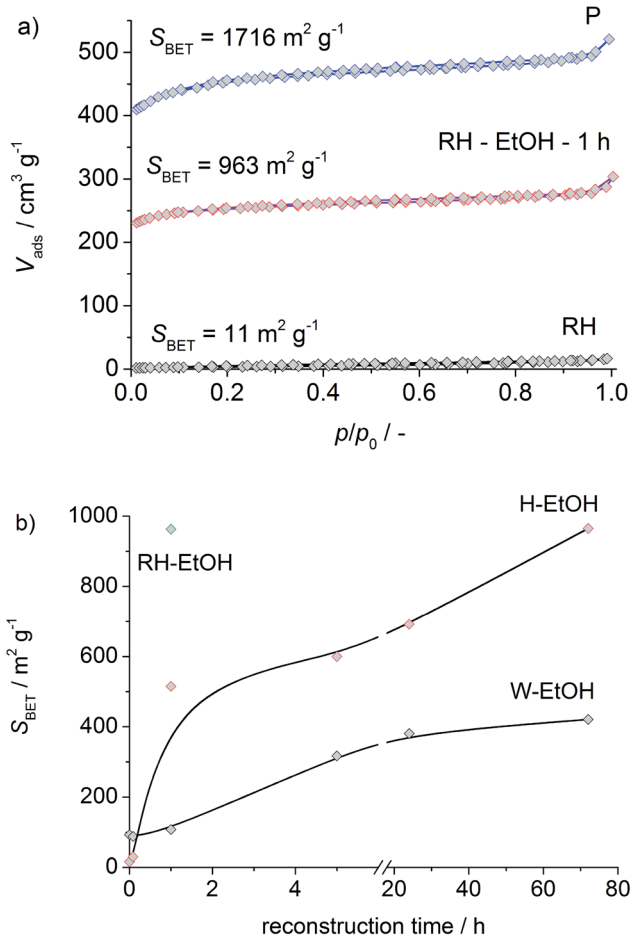

Figure 4. a) Representative N_2 isotherms of the reconstruction process for sample RH and b) evolution of the total surface area during reconstruction of degraded material obtained from different degradation routes.

no complete recovery of the surface area was achieved under the conditions applied, sample H-EtOH did not reach a plateau compared to sample W-EtOH.

2.2. In Situ Steaming and Reconstruction of HKUST-1 for Pre-Combustion CO_2 Capture

The simplicity of the reconstruction principle and the fact that the porosity of the material is not compromised by occluded additives compared to other methods,[29] bestow this approach a high degree of attractiveness for its application in processes that would require in situ reconditioning of the MOF material. Flue gas and biogas purification comprise one of the most important end applications envisioned for MOFs, e.g. in pre-combustion CO_2 capture, i.e. removal of carbon dioxide from the gas stream after the fossil fuel has been gasified and subsequently treated in a water-gas shift (WGS) reactor.[32] The high pressure (≤6.0 MPa) of the resulting H_2/CO_2 mixture and the high concentrations of CO_2 (≤50 mol.%)[33] justify a preferred application of physisorbents like MOFs, zeolites, or activated carbons. Due to its superior CO_2 uptake[14,18] and its excellent

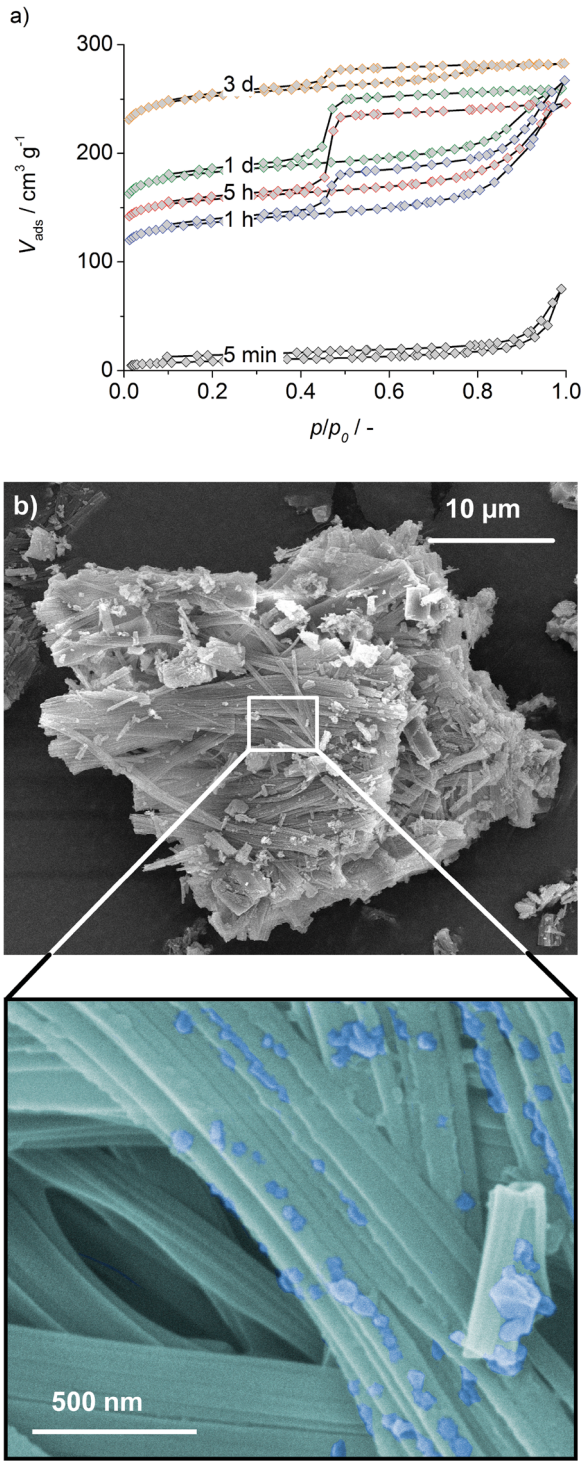

Figure 5. a) Nitrogen sorption isotherms during reconstruction of samples H in EtOH at 25 °C and b) false-colored, close up SEM image of the genesis of HKUST-1 crystals (blue) from the inside of a micrometer-sized crystal of sample H-EtOH after 5 min reconstruction (cyan).

H_2/CO_2 selectivity,[34] particularly HKUST-1 is a most suitable material for this application. However, even small amounts of water (≤1 mol.%) remaining after the WGS unit have the

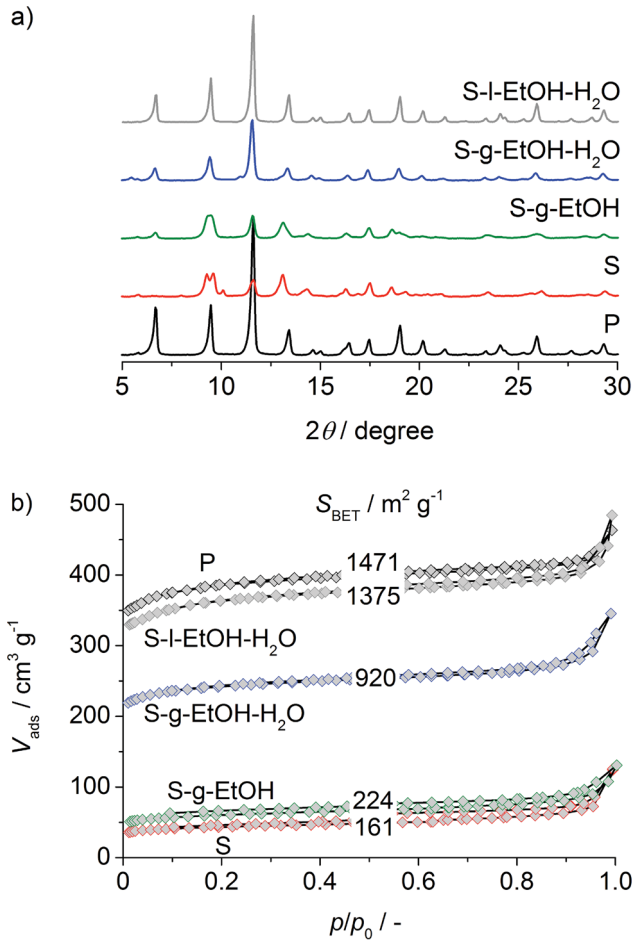

Figure 6. a) XRD patterns and b) corresponding N_2 isotherms of samples degraded and in situ reconstructed in a fixed-bed reactor. Data were recorded after complete removal of the solvents in the reactor (i.e. heating at 150 °C in a flow of N_2 for 1 h).

potential to compromise the MOF crystalline structure after prolonged exposure.[5,22]

We used a continuous fixed-bed reactor setup in order to evaluate the possibility of in situ line regeneration of HKUST-1 (see Table 1 for detailed treatment conditions). Taking into account that the reconstruction approach was deemed not to be governed by free, dissolved species, this is considered to be a valid comparison to the experiments described in Section 2.1. Rather harsh conditions for MOF materials (275 °C, 50 mol.% steam, 2 h) were applied for steaming degradation of pure pelletized (200–400 µm particle size) HKUST-1. Sample S showed a complete disappearance of the characteristic reflections for HKUST-1 (as can be easily monitored with the one at 6.7° 2θ), indicating the complete rearrangement of HKUST-1 into a different structure (**Figure 6**a). The effect in porosity for the steamed sample (S) turned out to be drastic, with an almost complete loss in total surface area down to 161 m^2 g^{-1}, 11% of the parent material (Figure 6b). HKUST-1 reconstruction experiments for CO_2 capture underwent optimization using gas streams of pure EtOH (sample S-g-EtOH) or a mixture of EtOH/H_2O (sample S-g-EtOH-H_2O), respectively. The combination of solvents was applied in order to favor reorganization into HKUST-1, emulating the original synthesis procedure.[26] All of which resulted in an optimized reconstruction recovering the initial phase (Figure 6a) and 15% (S-g-EtOH) and 50% (S-g-EtOH-H_2O) of the surface area, respectively (Figure 6b). The reconstructed material demonstrated high crystalline homogeneity along the entire reactor column, with only the upper (~0.5 cm) layer showing even higher degrees of reconstruction based on the S_{BET} value. Although thin-film condensation on the surface of the pellets cannot be discarded, no massive on-column condensation of solvent could be established, as no change in the morphology or size of the pellets was observed after in situ reconstruction in gas phase at all (see Supporting Information Figure S7). While the use of gas streams demonstrated the low solvent requirements of our approach, the beneficial features of a pure liquid treatment in a mixture of EtOH/H_2O (sample S-l-EtOH-H_2O) are evident: almost complete recovery of the entire crystallinity and up to 94% of the porosity in the same amount of time (5 h). This treatment was carried out at 70 °C in order to be as close as possible to the one in gas-phase operation. It should be noted that, under the conditions investigated in this work, steaming with an EtOH/H_2O stream did not hinder the collapse of HKUST-1 compared to pure steam, but the possibility of such a behavior under lower temperature conditions cannot be discarded. However, such a study would require far prolonged steaming experiments.

The CO_2 capacity of the differently-treated samples was determined in the same fixed-bed reactor by conducting breakthrough experiments using a mixture of H_2:CO_2 = 50:50 at 30 °C and 6.0 MPa (**Figure 7**a). The shape of the CO_2 curves is essentially the same for all tested materials (P, S, S-g-EtOH-H_2O, S-l-EtOH-H_2O), which means that the kinetics are not affected by degradation or reconstruction. However, a slight shift of the H_2 curve was noticed for the steamed sample S (Figure 7a inset). This could be explained by the presence of copper-oxo species, which might exhibit a weaker interaction with H_2 than the Cu nodes in the MOF structure due to more saturated metal centers; leading to a steeper breakthrough curve. Such effect is unlikely to be solely caused by changes in the surface area of the material. The degree of reconstruction, expressed as porosity, scales linearly with the calculated CO_2 uptake (Figure 7b), which is typical for physisorbents. Thus, not only the materials' properties are recovered, but also a great part of the sorption capacity is restored compared to the parent sample. During CO_2 sorption no production of carbonates from introduction into the degraded HKUST-1 structure was observed in XRD evaluations.

SEM imaging of the corresponding samples (Figure 7b insets) show that steaming itself results in the generation of particles exhibiting smoother crystalline features and large pores with a mean size of 80 nm. When regenerating HKUST-1 in gas phase EtOH/H_2O, the morphology of the crystals is a combination of what can be considered a reconstruction by both coverage of opened macropores and a deeper reconstruction of crystals similar to the typical octahedral morphology of the parent material. The latter is more pronounced by conversion in the liquid phase.

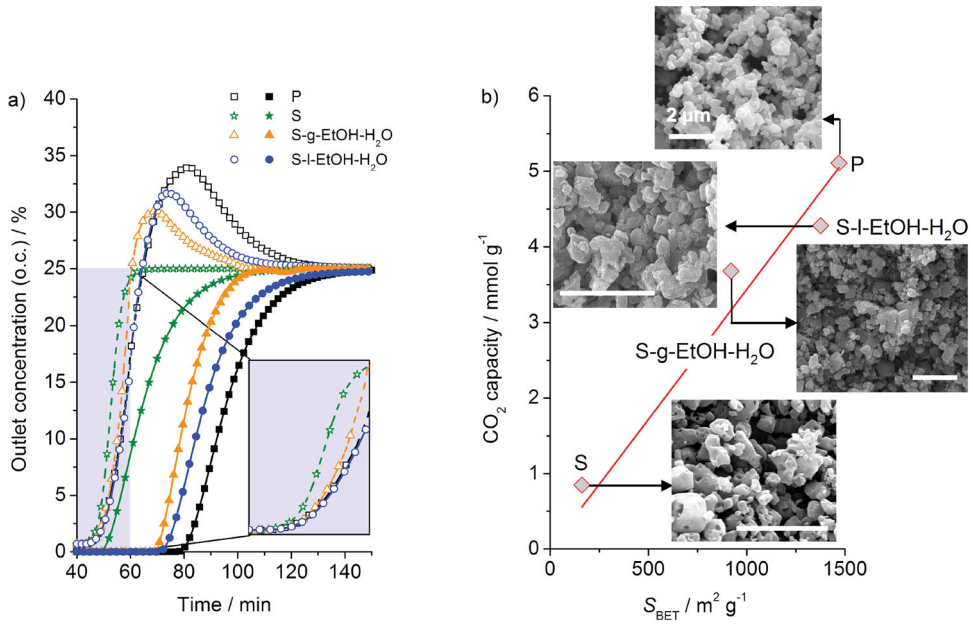

Figure 7. a) Breakthrough experiments of mixtures of H_2/CO_2 over HKUST-1 in different states: breakthrough curves of H_2 (open symbols) and CO_2 (filled symbols). Molar ratio H_2:CO_2 = 50:50, 30 °C, 6.0 MPa. Inset shows details of the H_2 breakthrough curves. b) CO_2 capacity in correlation with the total surface area. Corresponding scanning electron micrographs are shown as insets (scale bars correspond to 2 µm).

2.3. Degradation Mechanism and Influence in Reconstruction

The degradation mechanism of MOF materials, including HKUST-1, has recently gained attention. As mentioned before, stability values generally accompany most MOF reports, but Low et al., studying the modeling of MOF stability, have presented a mapping of steam stabilities and highlighted the conversion of MOFs into a material containing metal hydroxide and protonated linker.[7] Decoste et al. have also revisited the decomposition kinetics of different MOFs, including HKUST-1, under different temperature and humidity conditions providing some insight in the matter.[35] In our study, as concluded from XRD analysis, the degradation of the porous network of HKUST-1 followed different routes and resulted in different phases comparing prolonged exposure to humidity, high-temperature steaming or direct treatment with water or diluted acid. Infrared spectroscopy contributed to elucidate the entire process from framework collapse into a hybrid material to its reconstruction back to HKUST-1. The original experiment was particularly interesting for this study due to its mild conditions and high level of reconstruction from a completely collapsed structure. Fourier-transform IR spectra in **Figure 8**a and b show the different stages of the HKUST-1 degradation and reconstruction process in the OH and fingerprint region, respectively. As expected, there is an increase in intensity of water-related –OH species in the OH stretch region with the degradation of the structure (Figure 8a). However, this process does not result in the restoration of the original structural –OH stretch vibrations of $Cu(OH)_2$ (2578 and 3320 cm^{-1}). Likewise, –OH vibrations typically originating from pure, crystalline trimesic acid are absent. This points towards an utterly different ordering of both copper-oxo species and trimesic acid. Predictably, upon reconstruction the intensity of these broad –OH signals decreases but do not reach the previous intensity or fine structure of the parent MOF. Vibrations in the fingerprint region (Figure 8b) provide a closer look on the different interaction of trimesic acid during the process. Namely, it is important to note that despite the complete collapse of the HKUST-1 framework, the trimesic acid linker seems to be in isolated, but still partially coordinated positions, and does not form crystalline aggregates outside the degraded crystals by itself. This is mainly seen in the low intensity of C=O and C–OH vibrations (1718 and 1277 cm^{-1}, respectively), which are characteristic of decoordinated or partially coordinated trimesic acid, and is also seen in the two crystal structures found for sample H. Additionally, the larger number of $–CO_2$ vibrations arising between 1600 and 1500 cm^{-1}, related to the linker assuming a larger variety of environments,[36] upon collapse of the pore network, decrease but do not completely recede in the reconstructed product. C–H and C=C stretch vibrations (1454, 1404 cm^{-1}), from the aromatic structure of the linker, also reappear shifted upon degradation of the structure, but recede after reconstruction.

An insight into the high dependence of the level of reconstruction of HKUST-1 from the corresponding degradation methods can be provided by investigation of the different chemical environments that arise. The –OH stretch vibrations greatly differ between degradation methods (Figure 8c), for example steamed samples show a low number of –OH species generated but a loss of the fine structure of vibrations, closer to the sample produced through exposure to humidity. Liquid-treated samples are the ones who experience a more aggressive generation of water-related –OH species. While both, water and HCl-treated samples exhibit certain increase in the amount of these vibrations, the water-treated sample shows a closer chemical

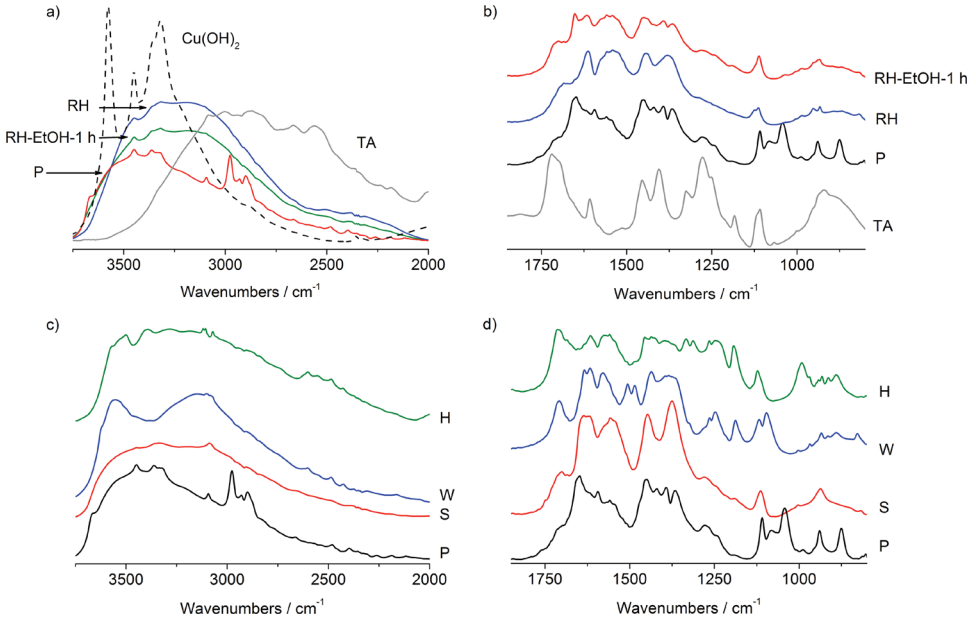

Figure 8. Infrared spectra analysis of a) OH region and b) fingerprint region of initial HKUST-1 reconstruction experiment and c) OH region and d) fingerprint region of differently degraded samples of HKUST-1.

resemblance to $Cu(OH)_2$, while the HCl-treated sample showed a markedly lower amount, accompanied by a loss of structural –OH vibrations. These differences, albeit obvious and expected, help to identify the importance of –OH species in the entire reconstruction process, which will be explained later in detail.

As suggested earlier, the reconstruction may well be explained by the formation of a hybrid material comprising an intimate mixture of TA and Cu species upon degradation, and thus the coordination and state of the linker is also of interest. Namely, the coordination of trimesic acid varies between different degradation methods. It is evident in Figure 8d, from the increase in the C=O and C–OH vibrations of samples H and W (1718 and 1277 cm^{-1} respectively) that a certain amount of trimesic acid is only partially coordinated in the structure (especially in view of structures H1 and H2). The exception is the steamed sample, which shows a remarkably low level of partially coordinated TA. Furthermore, the water-treated sample shows additional trimesic acid positions as a split signal at 1495 cm^{-1}. Decoordination of the TA brought by the degradation process is also present to a certain degree as C=O and C–OH vibrations in most of the reconstructed samples (Supporting Information, Figure S8). However, the presence of this small amount of disordered TA did not influence crystallinity, porosity or CO_2 uptake capacity.

Free, completely decoordinated TA can be mostly ruled out, even considering sample H, as its diffraction profile does not show any and TG-MS analysis only showed a minimal amount (Supporting Information, Figure S9), an effect related to Cu^{2+} removal during the degradation treatment by partial dissolution of the structure as seen in the TA:Cu ratios from the crystal structures H1 and H2. It should be noted that eventually formed oxygen-stabilized Cu-species (e.g. $Cu(OH)_2$) should not dissolve in diluted acid aqueous milieu due to their strong hydrophobicity and stabilization by TA. The changes in TA coordination observed by IR analysis of degraded materials are also not only present in the crystal structures of sample H, but finally reflected in the TG-MS profiles presenting differently coordinated TA species, observed as splitting of the CO_2 signal (corresponding to the decomposition of TA). In accordance to initial XRD structural observations of multiple phases, up to five different water species between 50–300 °C were present in sample W. This number is reduced to two main (130 and 240 °C) and a minority number of species (378 °C) in sample H and the steamed sample S shows only one (100 °C). All of the signals of adsorbed water and TA species eventually return to the original positions of the parent sample (H_2O: 90–100 °C, CO_2 (TA): 345 °C) for the samples that were successfully reconstructed (Supporting Information, Figure S10).

The above-presented observations enable us to suggest a mechanism for HKUST-1 degradation and how it influences the reconstruction procedure (**Figure 9**). An atmosphere with 77% relative humidity (sample RH) gently induces degradation of the framework by a gradual hydrolysis of individual linker-metal bonds, creating a low amount of water-related –OH sites. On the other hand, treatment with liquid water (sample W) induces hydrolysis of linkers but creates a greater number of –OH sites and a higher amount of decoordinated trimesic acid. In our case, it is reasonable to expect the greater amount of these sites to hydrophilize the resulting material, making a mobility and reorganization of trimesic acid molecules more difficult, compared to the material obtained under 77% RH. Furthermore, it is possible, regarding the partially corroded crystals, that the diffusion of the assisting solvent may be higher in the HCl-treated sample H by creation of additional macroporosity, which results in faster kinetics. Additionally, the non-excessive amount of –OH sites for sample H may well facilitate

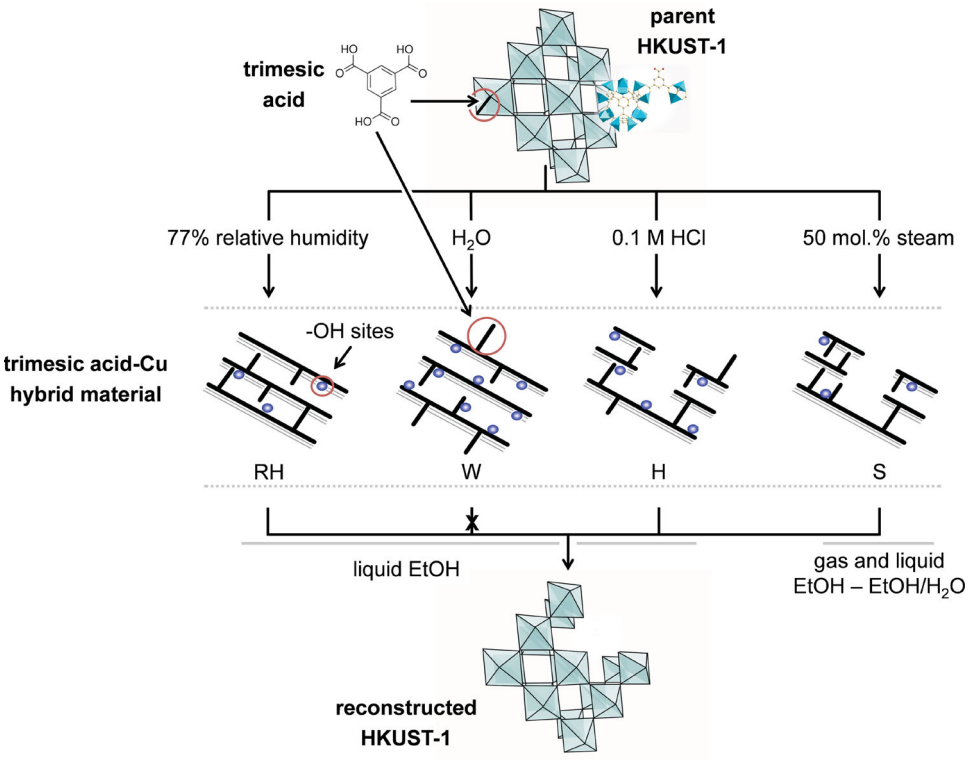

Figure 9. Schematic representation of the influence of different degradation approaches of HKUST-1 on the degraded materials and the subsequent reconstruction step.

TA mobility due to a positive effect of the moderate polarity in the material. Such an effect was demonstrated by Martín-Calvo et al., where a reasonable amount of water inside HKUST-1 is capable to facilitate the diffusion of molecules such as CCl_4.[37] An ideal combination of low trimesic acid decoordination, low amount of –OH sites and macropores also provide the sample S, obtained by steaming, favorable kinetics for the reconstruction into HKUST-1, which is further facilitated by the higher concentration of solvent in the liquid state experiment. Considering all this information and the crystal structures of sample H as a guideline, the use of EtOH and EtOH/H_2O mixtures would result in reconstruction by disturbing H-bonding between neighboring trimesic acid molecules. This would enhance their flexibility/mobility for coordination to nearby Cu atoms, which would in turn help to destabilize the polymeric Cu-O chains for facilitating successive reconstruction steps. The overall slower kinetics of the reconstruction, compared to the original synthesis of HKUST-1 from $Cu(OH)_2$,[26] are expected mainly due to the negative entropic effect of the degradation on the structure of the resulting hybrid materials. Compared to MOF recovery through dissolution and recrystallization using templating additives, which also block the accessible porosity,[29] the method presented here is not limited by the presence of species in solution or templates and thus a dissolution route is also not expected to be relevant for the reconstruction process, increasing its versatility. It is also interesting to note that this simple approach can cover different crystalline phases obtained from different degradation methods. This may well extend to other structures outside this study obtained using other degradation conditions, such as the one presented by Mustafa et al., which also present an interlayer distance of 3.5 Å.[15] Additionally, it should be mentioned that thin-film condensation on the particles as in the case of samples reconstructed in the gas phase may favorably contribute to the reconstruction. The extrapolation of this methodology to other structures has additionally a high probability to be generalized, even if some metals that agglomerate and/or oxidize (e.g. iron, aluminum) upon extraction from a MOF network may not be suitable for it. In fact, the observations of the impact of methanol on the surface of cobalt dioxidoterephthalate crystals, which may well be considered a solvent-assisted reconstruction of the structure, has been just recently reported by the team of Caro.[38]

3. Conclusions

We have demonstrated the water-related degradation of MOF materials to be actually reversible for the case of HKUST-1. Although the process is dependent on minimal amounts of solvent, liquid-phase treatments ultimately turned out to be the most effective one achieving up to 94% recovery of the material porosity. Extrapolation of the approach to a facile, single step in a fixed-bed reactor was also favorable for CO_2 capture. Furthermore, we have provided a rational mechanistic understanding of the entire process and possible variables affecting the reconstruction process.

The presented reconstruction principle has vital implications for the breakthrough of MOF materials into industrial applications. While certainly other stable MOF materials, have demonstrated also remarkable efficiency for CO_2 capture,[39] HKUST-1 now presents an ideal compromise of high CO_2 capture performance,[25] environmental friendliness, low-cost and high-productivity synthesis,[26] acceptable chemical and hydrothermal resistance.[7] And now, it finally exhibits the long sought missing link for closing the life-cycle for industrial application, a simple, effective and low-cost material reconstruction. In addition to enabling its reconditioning at early and late stages of degradation and contributing to dramatically lower expected operating costs for gas capture, this route also opens new venues for self-healing of MOF technical forms such as membranes and shaped bodies.

4. Experimental Section

Materials Synthesis and Procedures: The parent HKUST-1 material (P) was obtained through $Cu(OH)_2$ conversion.[26] Namely, using a thermostated (25°C), mechanically-stirred 5 L Multi-Purpose mini-plant pilot reactor from Büchiglas, 121.7 g trimesic acid (TA, 1,3,5-benzenetricarboxylic acid, ABCR Chemicals, 98%) was dissolved in 2.7 L ethanol. Thereafter, a suspension of 100 g $Cu(OH)_2$ (Aldrich, 56–57% Cu^{2+}) in 1 L deionized water was added, after homogenization by ultrasonication for 30 min, for achieving a reaction mixture of 3.7 L in total. The molar composition of the resulting mixture was 1 Cu^{2+}:1 TA:80 EtOH:100 H_2O. Approximately 280 g of pure HKUST-1 were recovered by filtration and drying after 1 h. Conditions for all degradation and reconstruction experiments are listed in detail in Table 1. In a typical degradation experiment, 4 g of HKUST-1 were added to 200 cm^3 distilled water (sample W) or 0.1 M HCl (sample H) heated to 85 °C under stirring. Samples were periodically collected, isolated by filtration, washed with water and ethanol, and then dried at 65 °C overnight. Only sample H experienced liberation of Cu^{2+} in solution and 40% loss of solid. For batch reconstruction, 1.25 g of dry, degraded HKUST-1 was added to 50 cm^3 ethanol and stirred at 25 °C (samples X-EtOH-t, e.g. H-EtOH-1 d). Samples were periodically taken, isolated by filtration, washed with ethanol and dried at 65 °C overnight. Pure material, pelletized (0.6 MPa, 30 s) and sieved fraction (200–400 μm), was used for in situ degradation and reconstruction in the gas phase. In this case, the samples were recovered in dry form from the reactor and evaluated as-obtained. For reconstruction in liquid phase, in situ degraded samples were recovered after reconstruction by filtration, washed only with water, dried at 65 °C and re-pelletized for CO_2 separation evaluation.

Characterization: The crystallization process and phase purity were monitored by powder X-ray diffraction obtained using Cu$K\alpha$ radiation in a PANalytical X'pert Pro diffractometer. The size and morphology of the obtained materials were determined by SEM in a FEI Quanta 200 F microscope. Nitrogen isotherms were measured in a Quantachrome Quadrasorb SI instrument after degassing the samples at 150 °C for 3 h. DRIFT spectra (10% in KBr) were collected in a Bruker Vertex 70 instrument (4 cm^{-1} resolution, 200 scans). Thermogravimetric measurements were carried out under a flow of air (40 cm^3 min^{-1}) and a heating rate of 10 °C min^{-1} in a Mettler Toledo STARe TGA instrument connected to a Pfeiffer Vacuum ThermoStar GSD 320 T1 Gas Analysis System for detecting gaseous products of thermal decomposition.

Structure Determination: Synchrotron X-ray powder diffraction data were collected on samples **H**, **W**, and **S** on the Materials Science beam line at the Swiss Light Source (wavelength 0.7085 Å, Mythen II detector). The diffraction pattern for **H** (Figure S3) showed two clearly distinct peak shapes, hinting at the presence of two possible phases. One of the phases (hereafter referred to as **H1**) possessed relatively narrow peaks, and could be indexed with a monoclinic cell ($P21/n$; $a = 6.841$ Å, $b = 18.851$ Å, $c = 8.565$ Å, $\beta = 92.869°$) using the indexing routine in the program TOPAS.[40] Intensity extraction was performed using the Pawley[41] fitting routine implemented in TOPAS.[40] Due to the presence of a strong scatterer (Cu), structure solution was relatively straightforward using the powder charge-flipping (*pCF*; [42] algorithm implemented in the program Superflip [43] with optimized parameters.[44] Two C atoms were missing, but could be added based on geometric considerations.

All the remaining Bragg peaks in the diffraction profile of **H** could be indexed with a monoclinic cell ($P21$; $a = 13.544$ Å, $b = 18.234$ Å, $c = 3.655$ Å, $\beta = 91.529°$). This cell was chosen, because the c parameter corresponds well with the interlayer distance found in **H1**. This second phase (hereafter **H2**) could not be solved directly using the *pCF* algorithm, and only yielded partial solutions. At best, the location of the Cu and some of the coordinated O atoms could be identified. Using this information, in combination with the fact that the TA molecules would probably be stacked along the *c*-axis, an initial model could be constructed. The structure was eventually solved by fixing the position of the Cu atoms and using the simulated annealing algorithm in *TOPAS* to find the orientation and location of the two independent TA molecules, which were added as rigid body models.

Rietveld refinement of the structures of **H1** and **H2** was performed using *TOPAS*. Restraints on the Cu–O distances were added where necessary and the TA molecules were refined as rigid body models, because the data would not allow refinement of the individual atoms. The background was removed manually and adjusted during the course of the refinement. Refinement is still in progress, and structures presented in this paper are preliminary. Crystallographic details of the refinement for **H** can be found in Table S1. The structure of **H1** was later identified to be equivalent to one reported by Pech and Pickardt (CSD code: VUXBUL).[45]

The diffraction pattern for **W** (Figure S4) could initially not be indexed with a single unit cell, indicating the possibility of multiple phases being present. Once the structure of **H1** was resolved, it was identified to be present as a minor phase in **W**. A second minor phase was identified as a layered $[Cu_2OH(BTC)(H_2O)]$ phase (CSD code: OHOMIH).[31] The remaining Bragg peaks for the third, most prominent phase can be indexed with a monoclinic cell that has also a cell parameter of 3.5Å, indicating a layered structure. However, attempts to solve the structure with *pCF* and simulated annealing have so far failed.

The diffraction pattern for **S** shows poor crystallinity. The pattern could not be indexed with a single unit cell. Possibly, **S** contains multiple phases, but attempts at indexing have failed so far and none of the previously discussed structures could be identified, but is is very likely that the phases will be different modifications (but chemically related) to the one present in phase **H**.

CO_2 Separation. Pure material, pelletized (0.6 MPa, 30 s) and sieved fraction (200–400 μm), was used for CO_2 sorption evaluation at pre-combustion capture conditions in a fixed-bed flow reactor. Prior to the experiment, the sorbent bed was activated at 150 °C for 1 h (5 °C min^{-1}) in He (GHSV = 600 h^{-1}). The CO_2 capacity was determined from the temporal difference of the breakthrough curves of H_2 and CO_2 monitored by an Omnistar GSD 301 mass spectrometer (Pfeiffer Vacuum). For this, the gas flow was switched to a molar composition of 50 He:25 H_2:25 CO_2 at 30 °C, 6.0 MPa, and GHSV = 200 h^{-1} (40 cm^3 min^{-1} total flow; 0.52 m s^{-1} linear velocity). Flow conditions have been adjusted in order to avoid radial and axial dispersion in the bed by using a high ratio of bed length over the diameter (~14) and a volumetric flow large enough to result in a relatively high ratio of advective transport rate over the diffusive one. Steaming and reconstruction conditions are detailed in Table 1. The dynamic CO_2 uptake was retrieved based on the temporal difference of the H_2 and the CO_2 curve (Δt), the molar inlet flow of CO_2 ($F(CO_2)$), and the mass of sorbent used ($m_{sorbent}$) (CO_2 capacity = Δt $F(CO_2)$ $m_{sorbent}^{-1}$).

Supporting Information

Supporting Information is available from the Wiley Online Library or from the author.

Acknowledgements

We thank Dr. K. Kunze at the Electron Microscopy Center ETH Zürich (EMEZ) for help with electron microscopy studies. S.S. gratefully acknowledges funding from the Swiss National Science Foundation and thanks the beamline scientists at the Swiss Light Source in Villigen, Switzerland, for their assistance with the powder diffraction measurements.

Received: October 29, 2013
Revised: December 12, 2013
Published online: February 20, 2014

[1] J.-R. Li, R. J. Kuppler, H.-C. Zhou, *Chem. Soc. Rev.* **2009**, *38*, 1477.
[2] J. L. C. Rowsell, O. M. Yaghi, *Micropor. Mesopor. Mater.* **2004**, *73*, 3.
[3] J. Lee, O. K. Farha, J. Roberts, K. A. Scheidt, S. T. Nguyen, J. T. Hupp, *Chem. Soc. Rev.* **2009**, *38*, 1450.
[4] P. Horcajada, R. Gref, T. Baati, P. K. Allan, G. Maurin, P. Couvreur, G. Férey, R. E. Morris, C. Serre, *Chem. Rev.* **2011**, *112*, 1232.
[5] S. Chaemchuen, N. A. Kabir, K. Zhou, F. Verpoort, *Chem. Soc. Rev.* **2013**, DOI: 10.1039/c3cs60244c.
[6] J. Gascon, F. Kapteijn, *Angew Chem., Int. Ed.* **2010**, *49*, 1530.
[7] J. J. Low, A. I. Benin, P. Jakubczak, J. F. Abrahamian, S. A. Faheem, R. R. Willis, *J. Am. Chem. Soc.* **2009**, *131*, 15834.
[8] T. Loiseau, C. Serre, C. Huguenard, G. Fink, F. Taulelle, M. Henry, T. Bataille, G. Férey, *Chem. Eur. J.* **2004**, *10*, 1373.
[9] K. S. Park, Z. Ni, A. P. Côté, J. Y. Choi, R. Huang, F. J. Uribe-Romo, H. K. Chae, M. O'Keeffe, O. M. Yaghi, *Proc. Natl. Acad. Sci. USA* **2006**, *103*, 10186.
[10] S. Marx, W. Kleist, J. Huang, M. Maciejewski, A. Baiker, *Dalton Trans.* **2010**, *39*, 3795.
[11] M. Savonnet, A. Camarata, J. Canivet, D. Bazer-Bachi, N. Bats, V. Lecocq, C. Pinel, D. Farrusseng, *Dalton Trans.* **2012**, *41*, 3945.
[12] Q. Yang, S. Vaesen, F. Ragon, A. D. Wiersum, D. Wu, A. Lago, T. Devic, C. Martineau, F. Taulelle, P. L. Llewellyn, H. Jobic, C. Zhong, C. Serre, G. De Weireld, G. Maurin, *Angew Chem., Int. Ed.* **2013**, *52*, 10316.
[13] J. B. Decoste, G. W. Peterson, M. W. Smith, C. A. Stone, C. R. Willis, *J. Am. Chem. Soc.* **2012**, *134*, 1486.
[14] Q. A. Wang, J. Z. Luo, Z. Y. Zhong, A. Borgna, *Energy Environ. Sci.* **2011**, *4*, 42.
[15] D. Mustafa, E. Breynaert, S. R. Bajpe, J. A. Martens, C. E. A. Kirschhock, *Chem. Commun.* **2011**, *47*, 8037.
[16] S. J. Yang, C. R. Park, *Adv. Mater.* **2012**, *24*, 4010.
[17] X. Liu, M. Park, S. Hong, M. Oh, J. W. Yoon, J.-S. Chang, M. S. Lah, *Inorg. Chem.* **2009**, *48*, 11507.
[18] S. Choi, J. H. Drese, C. W. Jones, *ChemSusChem* **2009**, *2*, 796.
[19] M. Gaab, N. Trukhan, S. Maurer, R. Gummaraju, U. Müller, *Micropor. Mesopor. Mater.* **2012**, *157*, 131.
[20] L. Bellarosa, J. M. Castillo, T. Vlugt, S. Calero, N. López, *Chem. Eur. J.* **2012**, *18*, 12260.
[21] I. Bezverkhyy, G. Ortiz, G. Chaplais, C. Marichal, G. Weber, J.-P. Bellat, *Micropor. Mesopor. Mater.* **2014**, *183*, 156.
[22] D. M. D'Alessandro, B. Smit, J. R. Long, *Angew Chem., Int. Ed.* **2010**, *49*, 6058.
[23] J. B. DeCoste, G. W. Peterson, H. Jasuja, T. G. Glover, Y.-g. Huang, K. S. Walton, *J. Mater. Chem. A* **2013**, *1*, 5642.
[24] G. W. Peterson, G. W. Wagner, A. Balboa, J. Mahle, T. Sewell, C. J. Karwacki, *J. Phys. Chem. C* **2009**, *113*, 13906.
[25] L. Hamon, E. Jolimaître, G. D. Pirngruber, *Ind. Eng. Chem. Res.* **2010**, *49*, 7497.
[26] G. Majano, J. Pérez-Ramírez, *Adv. Mater.* **2013**, *25*, 1052.
[27] G. Majano, O. Ingold, M. Yulikov, G. Jeschke, J. Pérez-Ramírez, *CrystEngComm* **2013**, *15*, 9885.
[28] Z. Chen, G. Wang, Z. Xu, H. Li, A. Dhôtel, X. C. Zeng, B. Chen, J.-M. Saiter, L. Tan, *Adv. Mater.* **2013**, *25*, 6106.
[29] N. Janssens, L. H. Wee, S. Bajpe, E. Breynaert, C. E. A. Kirschhock, J. A. Martens, *Chem. Sci.* **2012**, *3*, 1847.
[30] A. Pöppl, B. Jee, M. Icker, M. Hartmann, D. Himsl, *Chem. Ing. Tech.* **2010**, *82*, 1025.
[31] J. Chen, T. Yu, Z. Chen, H. Xiao, G. Zhou, L. Weng, B. Tu, D. Zhao, *Chem. Lett.* **2003**, *32*, 590.
[32] Intergovernmental Panel on Climate Change Special Report on Carbon Dioxide Capture and Storage (Eds: B. Metz, O. Davidson, H. de Coninck, M. Loos, L. Meyer), Cambridge University Press, Cambridge 2005, pp.442.
[33] J. D. Figueroa, T. Fout, S. Plasynski, H. McIlvried, R. D. Srivastava, *Int. J. Greenhouse Gas Control* **2008**, *2*, 9.
[34] B. Silva, I. Solomon, A. M. Ribeiro, U. H. Lee, Y. K. Hwang, J.-S. Chang, J. M. Loureiro, A. E. Rodrigues, *Sep. Purif. Technol.* **2013**, *118*, 744.
[35] J. B. Decoste, G. W. Peterson, B. J. Schindler, K. L. Killops, M. A. Browe, J. J. Mahle, *J. Mater. Chem. A* **2013**, *1*, 11922.
[36] R. J. Davey, M. Brychczynska, G. Sadiq, G. Dent, R. G. Pritchard, *CrystEngComm* **2013**, *15*, 856.
[37] A. Martin-Calvo, E. Garcia-Perez, A. Garcia-Sanchez, R. Bueno-Perez, S. Hamad, S. Calero, *Phys. Chem. Chem. Phys.* **2011**, *13*, 11165.
[38] C. Chmelik, A. Mundstock, P. D. C. Dietzel, J. Caro, *Micropor. Mesopor. Mater.* **2014**, *183*, 117.
[39] K. Sumida, D. L. Rogow, J. A. Mason, T. M. McDonald, E. D. Bloch, Z. R. Herm, T.-H. Bae, J. R. Long, *Chem. Rev.* **2011**, *112*, 724.
[40] A. A. Coelho, TOPAS-ACADEMIC v5.0. **2012**.
[41] G. Pawley, *J. Appl. Crystallogr.* **1981**, *14*, 357.
[42] C. Baerlocher, L. B. McCusker, L. Palatinus, *Z. Kristallogr.- Cryst.. Mater.* **2007**, *222*, 47.
[43] L. Palatinus, G. Chapuis, *J. Appl. Crystallogr.* **2007**, *40*, 786.
[44] D. Sisak, C. Baerlocher, L. B. McCusker, C. J. Gilmore, *J. Appl. Crystallogr.* **2012**, *45*, 1125.
[45] R. Pech, J. Pickardt, *Acta Crystallogr., Sect. C: Cryst. Struct. Commun.* **1988**, *44*, 992.